

# Elucidating Surface Ligand-Dependent Kinetic Enhancement of Proteolytic Activity at Surface-Modified Quantum Dots

Sebastián A. Díaz,<sup>†,§,▲,Ⓛ</sup> Soumyo Sen,<sup>||,▲</sup> Kelly Boeneman Gemmill,<sup>†</sup> Carl W. Brown, III,<sup>†,¶</sup> Eunkeu Oh,<sup>‡,∇</sup> Kimihiro Susumu,<sup>‡,∇</sup> Michael H. Stewart,<sup>‡</sup> Joyce C. Breger,<sup>†</sup> Guillermo Lasarte Aragonés,<sup>†,¶</sup> Lauren D. Field,<sup>†,⊗</sup> Jeffrey R. Deschamps,<sup>†</sup> Petr Král,<sup>\*,||,⊥,#,Ⓛ</sup> and Igor L. Medintz<sup>\*,†,Ⓛ</sup>

<sup>†</sup>Center for Bio/Molecular Science and Engineering, Code 6900, <sup>‡</sup>Optical Sciences Division, Code 5600, U.S. Naval Research Laboratory, Washington, D.C. 20375, United States

<sup>§</sup>American Society for Engineering Education, Washington, D.C. 20036, United States

<sup>||</sup>Department of Chemistry, <sup>⊥</sup>Department of Physics, <sup>#</sup>Department of Biopharmaceutical Sciences, University of Illinois at Chicago, Chicago, Illinois 60607, United States

<sup>¶</sup>College of Science George Mason University, Fairfax, Virginia 22030, United States

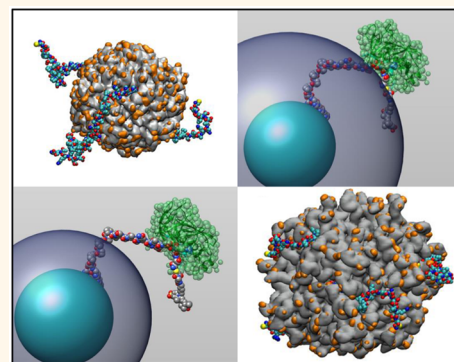
<sup>∇</sup>Sotera Defense Solutions, Inc., Columbia, Maryland 21046, United States

<sup>⊗</sup>Fischell Department of Bioengineering, University of Maryland, College Park, Maryland 20742, United States

## Supporting Information

**ABSTRACT:** Combining biomolecules such as enzymes with nanoparticles has much to offer for creating next generation synergistically functional bionanomaterials. However, almost nothing is known about how these two disparate components interact at this critical biomolecular-materials interface to give rise to improved activity and emergent properties. Here we examine how the nanoparticle surface can influence and increase localized enzyme activity using a designer experimental system consisting of trypsin proteolysis acting on peptide-substrates displayed around semiconductor quantum dots (QDs). To minimize the complexity of analyzing this system, only the chemical nature of the QD surface functionalizing ligands were modified. This was accomplished by synthesizing a series of QD ligands that were either positively or negatively charged, zwitterionic, neutral, and with differing lengths. The QDs were then assembled with different ratios of dye-labeled peptide substrates and exposed to trypsin giving rise to progress curves that were monitored by Förster resonance energy transfer (FRET). The resulting trypsin activity profiles were analyzed in the context of detailed molecular dynamics simulations of key interactions occurring at this interface. Overall, we find that a combination of factors can give rise to a localized activity that was 35-fold higher than comparable freely diffusing enzyme–substrate interactions. Contributing factors include the peptide substrate being prominently displayed extending from the QD surface and not sterically hindered by the longer surface ligands in conjunction with the presence of electrostatic and other productive attractive forces between the enzyme and the QD surface. An intimate understanding of such critical interactions at this interface can produce a set of guidelines that will allow the rational design of next generation high-activity bionanocomposites and theranostics.

**KEYWORDS:** enzyme, quantum dot, Michaelis–Menten, catalysis, nanotechnology



The promise driving much of the current research into bionanotechnology is directly predicated on the ability of functional composites assembled from both biological and nanomaterials to work together synergistically and provide emergent capabilities unavailable to each component independently.<sup>1–4</sup> Although the library of available nanomaterials is

continuously expanding and is quite diverse, the central workhorse material in this regard continues to be primarily

Received: March 7, 2017

Accepted: May 30, 2017

Published: June 12, 2017

centered around nanoparticles (NPs).<sup>5–9</sup> Along with common attributes such as high surface-to-volume ratios and the ability to act as a centralized nanoscaffold for chemical attachment, NPs can contribute value-added functionalities to these composites including photoluminescence (PL), magnetism, plasmonics, and the like.<sup>5–10</sup> It is the combination of these properties when married to biological functionalities such as binding specificity, targeting, catalysis, sensing, structural organization, *etc.*, that provides the added value or synergy to these hybrids.<sup>7</sup> Various applications are envisioned for these materials including stand-alone biosensors, light harvesting and biocomputing devices, along with theranostics, the latter of which provides perhaps one of the more illustrative concepts reflecting the longer-term possibilities. For example, within a putative oncological theranostic device, the NP could provide MRI or other *in vivo* contrast while simultaneously acting as a central scaffold to host biologicals such as antibodies for tumor targeting, peptides for facilitated cellular uptake, and poorly soluble chemotherapeutics for specified delivery.<sup>11,12</sup>

Some types of biologically functionalized NPs, such as antibody-decorated gold colloids, have now been in use for several decades,<sup>7</sup> however, it is only recently that the promise and the complexity of such hybrid materials have started to be fully realized. The latter is exemplified by the many requirements surrounding the optimal assembly of these composite materials including: (i) NP synthesis, (ii) surface functionalization, and (iii) bioconjugation. Ideally, the NPs should be uniform both chemically and structurally along with being almost monodisperse in size. Most (metallic) NPs have to be stabilized as colloids to be functional within biological environments since they do not possess any intrinsic solubility of their own. This requires use of so-called NP “ligands” which bind to or otherwise associate with the NP surface while providing colloidal stability through charge or other chemical functionalities such as poly(ethylene glycol) or PEG.<sup>7,13</sup> Available ligand classes are quite diverse and range from small discrete thiolated acids to large amphiphilic polymers. Along with the stabilizing ligands, for optimal activity biomolecular-NP composites require that the biological (*e.g.*, protein, peptide, DNA, *etc.*), be displayed on the NP with intimate control over orientation, ratio and separation distance among other properties.<sup>4,7,13</sup> Significant investments have and continue to be made in these three related areas and, as the resulting biocomposite assemblies have rapidly matured, it is here that previously unanticipated properties have been unexpectedly revealed beyond those that were initially desired.

Such emergent properties are perhaps best epitomized by the interfacing of NPs with enzymes which was originally undertaken in pursuit of more-stable biosensors, biocatalytic nanomaterials and replacement therapeutics as some illustrative examples.<sup>14–16</sup> Here, it was found that in many, but not all cases, enzymatic activity was enhanced at the NP interface regardless of whether it was the enzyme or the substrate attached to the NP. Examples of some of the enzymes that have demonstrated enhancement when attached to NPs include glucose oxidase, amylase, chymotrypsin, lipase, aldolase, and cholesterol oxidase, see refs<sup>14–16</sup> and therein for further examples. Since enzymatic enhancement at a NP interface has only been recently observed, the mechanism(s) that give rise to these phenomena are mostly unknown and have been variously ascribed to conformational changes, shielding, the NP microenvironment, confinement, optimized substrate trajectories, and colocalization.<sup>14–16</sup> Our previous work with various enzyme-NP systems suggested that different mechanisms contribute to enhancement within each of the experimental systems. Attaching alkaline phosphatase to

semiconductor quantum dots (QDs) in a controlled-oriented manner increased activity 20–40% above enzyme alone in contrast to a loss of activity when attached to the same type of NPs in a heterogeneous manner.<sup>17</sup> Similarly, attaching phosphotriesterase to QDs increased its initial catalytic rate ~4-fold and its enzymatic efficiency ( $k_{\text{cat}}/K_{\text{M}}$ ) ~2-fold. Here, the higher activity when attached to QDs was correlated with an acceleration in enzyme–product dissociation which is the enzyme’s putative rate limiting step. Decorating the tetrameric, diffusion-limited  $\beta$ -galactosidase enzyme with QDs also increased its catalytic rate 3-fold and, in this case, enhancement was suggested to occur due to substrate accumulation around the QD-enzyme assembly.<sup>18</sup> Lastly, in a converse configuration where a dye-labeled peptide substrate was assembled around QDs and exposed to trypsin, a “hopping” mechanism was postulated to give rise to up to 5-fold increases in enzyme efficiency.<sup>19</sup> In this modality, trypsin encountered a given labeled QD and rapidly consumed all the peptide surrounding it before diffusing away to the next interaction. Increased proteolytic activity for such substrate display on NPs has now been confirmed with several other enzymes.<sup>20–22</sup> Critically, the nanoscale confines and nature of the NP-enzyme interface where these enhancements occur remains almost completely undefined. It is believed to be characterized by boundary and phase separations, ionic and pH gradients along with structuring of the surrounding water among other localized properties.<sup>23,24</sup> Complicating this even more is that there are almost no analytical techniques available to directly probe this interfacial environment.

Although all components including the NP itself, the biomolecule and the localized environment will all contribute to the NP-biomolecular interfacial environment in a very complex manner, it is perhaps the surface ligands that are expected to be most defining here and indeed this has been already shown to some extent with gold NPs.<sup>25–35</sup> Surface ligands provide colloidal stability and typically bridge from the NP surface to the bulk environment while also having simultaneous contact with any attached biomolecules. With an aim toward understanding the critical role that NP surface ligands can play in enhancing enzymatic activity, we appropriate the aforementioned QD-peptide trypsin sensor and perform assays where only one variable is changed, namely the chemistry of the QD surface ligand, see Figure 1. Trypsin activity profiles were collected from QD-peptide assemblies capped with different ligand types and subsequently analyzed in conjunction with molecular dynamics simulations of key interactions occurring at this interface. Results suggest that a configuration where peptide substrate is prominently displayed extending from the QD surface in conjunction with strong attractive forces between enzyme and the QD surface can increase localized trypsin activity 35-fold or even higher.

## RESULTS AND DISCUSSION

### Quantum Dots, Peptide Substrate, and Assay Format.

The assay that forms the basis of this study is nearly identical to that previously described.<sup>19</sup> As highlighted in the schematic shown in Figure 1A, 520 nm emitting CdSe/ZnS QDs with a diameter of ~5.3 nm, (representative TEM in the Supporting Information, SI) were self-assembled with various discrete ratios of Cy3-labeled trypsin substrate peptide, the QD-peptide constructs exposed to trypsin in 1× phosphate buffered saline (PBS) and the resulting proteolytic activity monitored by the changes between the QD donor and Cy3 acceptor FRET. Quantitative analysis of the resulting data provides information

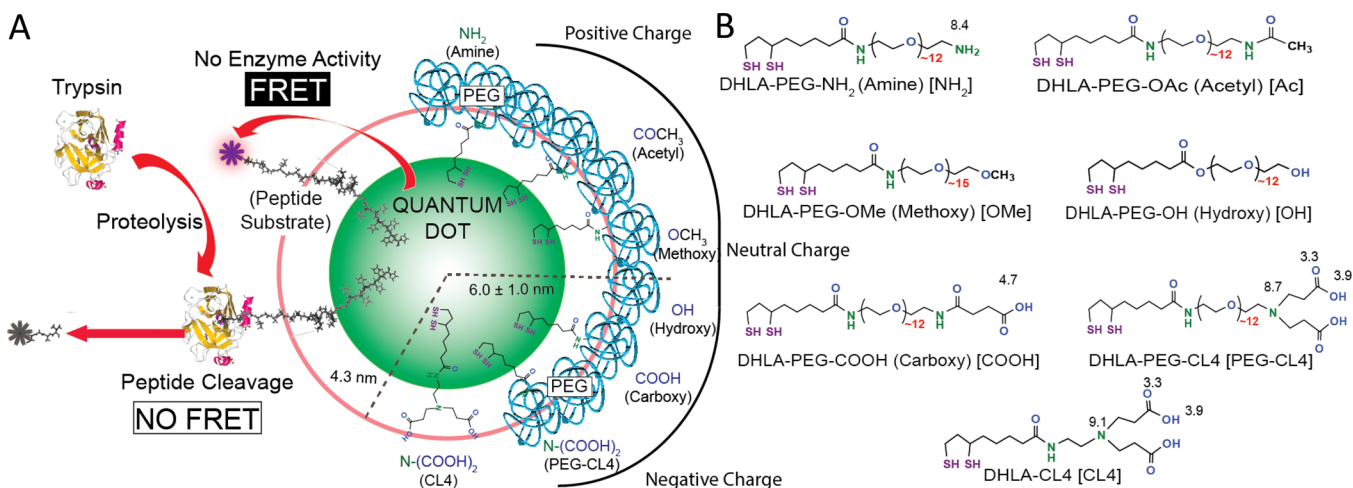


**Figure 1.** Schematic of the QD-dye-labeled peptide assemblies used for trypsin sensing (A) with the chemical structures of the 7 surface ligands tested (B). The terminal Cy3-labeled peptide is self-assembled to the QD through a  $(\text{His})_6$ -tag driven metal affinity coordination giving rise to a ratiometric FRET signal. In trypsin assays, multiple peptides are generally bound on average to a single QD species. In the presence of trypsin, the peptide is cleaved and the Cy3 dye will diffuse away from the QD modifying the FRET efficiency. The putative core/shell/ligand radii of QDs capped with the CL4 ligand and the PEGylated ligands are also shown at top to the most negatively charged (determined by  $\zeta$ -potential) at the bottom. The CL4 capped QD has a hydrodynamic diameter ( $H_D$ ) of 8.5 nm as compared to the PEGylated ligands which have larger  $H_D$ 's ( $\sim 11$ – $13$  nm) as measured by DLS (Table 1). The nominal number of ethylene oxide repeats is shown for each PEGylated ligand along with the  $pK_a$  of selected functional groups where available. The acetyl displaying ligand is part of an acetamide group. Not to scale.

on how the enzyme performs when the QD is surface-functionalized with different ligands presenting different chemical functional groups at the site of trypsin-peptide interactions.

The peptide utilized here is identical to the previous ( $N$ -\*CSTRIDEANQAATSLP<sub>7</sub>SH<sub>6</sub>-COOH where Cy3 is attached to the cysteine thiol\*) and contains four “modules” within its sequence which are meant to provide different utility: the  $N$ -terminal cysteine-thiol provides a specific chemical site for maleimide-based acceptor dye labeling; the STRIDEANQAAT portion contains a single arginine residue which trypsin recognizes and cleaves on its  $C$ -terminal side, as noted previously—this portion of the sequence can assume a highly bent or kinked structure;<sup>19</sup> the SLP<sub>7</sub>S is meant to form a type II polyprolyl helix that allows this sequence to function as a  $\sim 14$  Å spacer to direct the rest of the peptide away from the QD surface;<sup>36</sup> and the terminal  $(\text{His})_6$  motif attaches to the ZnS surface of the QDs. The latter bioconjugation is driven by high affinity metal coordination ( $K_d \approx 1$  nM) and is almost spontaneous when the peptide and QD are mixed together.<sup>37</sup> Although such self-assembly to QDs is characterized by a Poisson based process, it still provides for control over the average number of peptides assembled per QD which is critical to these assays. It is also important to note that, as reflected in several recent studies, the nature of the Poisson assembly does not detrimentally affect proteolytic assays implemented with these materials nor the ability to convert the observed FRET changes into enzymatic velocity.<sup>19–21,38</sup>

As outlined in the Experimental Section and described in detail previously,<sup>19</sup> self-assembly of the Cy3-labeled trypsin substrate to a green  $\sim 520$  nm emitting QD will promote FRET from the excited state QD donor to the Cy3 acceptor resulting in quenching and sensitization, respectively. Trypsin addition results in cleavage of the peptide which changes the rate of FRET in a manner proportional to the amount of enzyme activity. The resulting changes in FRET efficiency ( $E$ ) within this system can then be correlated to the amount of peptide cleaved

by comparison to a calibration curve consisting of an increasing ratio of dye-labeled peptide per QD versus FRET  $E$ ; in practice this is more easily implemented using the Cy3 acceptor/QD donor PL ratio. The amount of trypsin substrate cleaved over time can then be used to derive the enzymatic velocity or proteolytic rate. Although the trends will remain the same, for accurate, quantitative conversion using this approach, it is important to account for the effects of any nonspecific interactions of the dyes with the QD by using a true mix of cleaved and uncleaved peptides in the calibration curve as described before.<sup>19,21,22</sup> The combination of NP-displayed substrates and certain enzymes such as trypsin also require a specialized assay configuration to be implemented. The trypsin utilized here has a  $K_M$  of  $\sim 400$   $\mu\text{M}$ ,<sup>19</sup> which would require NP-peptide substrates in mM concentration to meet excess substrate, initial velocity conditions ( $>10\times K_M$ ) under standard Michaelis–Menten and Briggs–Haldane assumptions.<sup>39</sup> However, mM concentrations of NPs and especially QDs in buffer are not a physically achievable reality. Rather, an alternate integrated version of the Michaelis–Menten (MM) analysis is implemented where substrate (QD-trypsin peptide) is held constant and trypsin concentration is varied; these give rise to so-called enzymatic “progress curves” that are collected over extended time periods. We note that this same format and analytical approach was utilized by Michaelis and Menten in their seminal work.<sup>40</sup>

Two important caveats come with the use of this assay format. In the first, Selwyn’s test dictates that the progress curves from these formats should all superimpose when time is scaled by enzyme concentration,  $[E]_0$ , to yield a series of common trajectories in “enzyme time” ( $[\text{trypsin}] \times \text{time}$ ) only when the system is displaying Michaelis–Menten behavior.<sup>19,41</sup> Most simplistically, enzyme time represents substrate consumption as a function of the time the reaction has progressed multiplied by the enzyme concentration. Second, when the substrate concentration at time zero,  $[S]_0$ , is not greater than  $3\times$  the enzyme’s  $K_M$  ( $[S]_0 > 3K_M$ ), then fitting the progress

curves with the integrated form of the MM equation (eq 3 in the Methods) will only reflect the  $k_{\text{cat}}/K_{\text{M}}$  ratio. Nevertheless, this ratio is an effective second-order rate constant that describes enzyme efficiency and is sometimes referred to as the specificity constant. It is this metric that is compared across materials in the current study. We note that enzyme efficiency is particularly suited to comparing formats where the enzyme is unchanged and it is merely the substrate or its presentation that is modified in assays.<sup>42</sup> Higher  $k_{\text{cat}}/K_{\text{M}}$  values should correlate to more efficient systems with improved kinetics.

**Quantum Dot Surface Functionalizing Ligands.** In reduction to experiment, the QDs were self-assembled with several distinct ratios of peptide substrate and then assayed against increasing concentrations of trypsin, see Figure 1A. The main variable between each of these assays is the presence of a different surface functionalizing ligand on the QD. The different ligands are meant to alter the substrate's localized environment and presentation and hence the nature of the trypsin's interaction with the QD-peptide composite. To minimize all other variables while allowing us to isolate and probe the effect of just differences in QD surface chemistry, the same core ligand chemistry was utilized while varying either the functional groups displayed at the ligands termini or their lengths. Along with being synthetically feasible, this approach minimizes ligand density effects as well as the complexity that would be subsequently introduced by using ligands which are dramatically different from each other structurally, for example large amphiphilic encapsulating polymers versus discrete small thiolated acids.<sup>13,43,44</sup>

Figure 1B shows the structures of the QD surface ligands tested while Table 1 lists some pertinent characteristics of the QDs and QD-peptide assemblies when functionalized with these ligands. Where available in Figure 1B, the predicted  $\text{pK}_{\text{a}}$  of selected carboxyl and amine groups on the ligand's termini are also shown. Ligand synthesis and subsequent QD preparation with them are described in the SI. All the ligands consist of a dithiol binding motif which is provided by the dihydrothiolic acid (DHHLA) precursor. The bidentate thiols bind to the QD surface strongly and helps contribute to QD dispersions that are stable in aqueous solutions for long periods of time by alleviating many of the issues associated with the dynamic off-rate that monothiolated ligands typically experience.<sup>13,43,45</sup> The majority of the ligands then display a poly(ethylene glycol) or PEG linker of  $\sim 13$  ethylene oxide repeats except for the methoxy ligand which has  $\sim 16$  repeats. PEG is the preferred molecule for mediating colloidal stability in many established and developing NP and nanomedicine applications due to it is generally accepted

hydrophilic, inert and nonfouling character.<sup>46–49</sup> The ligand set then terminates in different functional groups including an amine ( $\text{NH}_2$ ), acetyl ( $\text{COCH}_3$ ), methoxy (OMe), hydroxy (OH), carboxy ( $\text{COOH}$ ), and zwitterionic group (CL4/PEG-CL4), see Figure 1 and Table 1. These names/designations are used somewhat interchangeably throughout. The zwitterionic ligands also came in two further length derivatives, a short compact ligand 4 (CL4), which is essentially just the DHHLA attached to a zwitterionic end group, and a PEGylated version of this ligand.<sup>43</sup> The amine, acetyl, hydroxy, and carboxy ligands all have the exact same structure except for the end group while the CL4 and PEG-CL4 have the same end groups and QD binding domain with the latter having a PEG linker separating them. As highlighted by the  $\zeta$ -potential results in Table 1 from QDs displaying these ligands, the CL4, PEG-CL4, and COOH QDs have strong negative charges, the OH QDs are only slightly negative, the OMe and  $\text{COCH}_3$  are neutral and the  $\text{NH}_2$  QDs are positively charged. The OMe and  $\text{COCH}_3$  ligands are also considered somewhat hydrophobic.

**Spectral Overlap, Peptide Extension and Quantum Dot Hydrodynamic Diameter.** Figure 2A shows the 520 nm emitting QD donor and Cy3 acceptor absorbance and emission profiles as normalized to quantum yield and this gives rise to the spectral overlap shown in Figure S2, which, in turn, gives rise to an estimated Förster distance or  $R_0$  of  $\sim 5.25$  nm. The representative plots shown in Figure 2B,C are collected from assembling the indicated increasing ratio of Cy3 acceptor-labeled peptide onto the QDs functionalized with either the small zwitterionic CL4 ligand or its larger related PEGylated derivative, respectively. The quenching of QD donor PL and sensitization of the Cy3 acceptor occurs in a manner that directly tracks the Cy3/QD ratio and is clearly visible in these FRET “titrations”. The inset in each plots this ratio versus FRET  $E$  as directly estimated from QD donor PL loss. Data collected in these plots serves two purposes. First, it acts as the aforementioned calibration curve that correlates changes in  $E$  with trypsin activity allowing us to estimate enzymatic velocity for each QD construct within a proteolytic assay. Second, using this data along with eq 1 in the Methods, we can estimate average QD donor center to Cy3 acceptor center separation distances ( $r_{\text{DA}}$ ), these are also listed in Table 1. Although not fully reflective of the final peptide conformation, especially if there is some twisting or kinking present within it, this measurement still provides information on how far from the QD surface the Cy3 acceptor itself is located; these estimates are also listed in Table 1. Interestingly, the CL4 ligand, which is the smallest of all the ligands tested here provides

**Table 1. Selected Characteristics of the Quantum Dots Displaying the Different Surface Ligands**

ligand <sup>a</sup>	abbr.	properties of interest ( $\sim$ MW)	$H_{\text{D}}$ [nm] <sup>b</sup>	$\zeta$ -potential [mV] <sup>c</sup>	QD-Cy3 $r_{\text{DA}}$ [nm] <sup>d</sup>
DHHLA Compact Ligand 4	CL4	Short, zwitterionic (394.6)	$8.5 \pm 0.4$	$-32.4 \pm 1.4$	$6.9 \pm 0.3$ (4.2/2.65)
DHHLA-PEG <sub>600</sub> -CL4	PEG-CL4	Long, zwitterionic (923.2)	$12.8 \pm 2.8$	$-28.2 \pm 1.6$	$5.8 \pm 0.2$ (3.1/–0.6)
DHHLA-PEG <sub>600</sub> -COOH	COOH	Long, negative charge (879.1)	$11.5 \pm 2.3$	$-24.7 \pm 1.1$	$6.2 \pm 0.2$ (3.5/0.45)
DHHLA-PEG <sub>600</sub> -OH	OH	Long, neutral (781.0)	$12 \pm 3$	$-7.3 \pm 0.9$	$5.9 \pm 0.2$ (3.2/–0.1)
DHHLA-PEG <sub>750</sub> -OMe	OMe	Long, hydrophobic (926.2)	$11.3 \pm 2.4$	$-2.9 \pm 0.4$	$6.2 \pm 0.2$ (3.5/0.55)
DHHLA-PEG <sub>600</sub> -Acetyl	Ac	Long, hydrophobic (821.1)	$12.4 \pm 3.2$	$0.4 \pm 0.3$	$5.6 \pm 0.3$ (2.9/–0.6)
DHHLA-PEG <sub>600</sub> -NH <sub>2</sub>	NH <sub>2</sub>	Long, positive charge (779.1)	$10.9 \pm 2.2$	$21.3 \pm 0.8$	$6.2 \pm 0.2$ (3.5/0.75)

<sup>a</sup>600/750 designates the approximate MW of the poly(ethylene glycol). <sup>b</sup>Hydrodynamic diameter of the QD surface functionalized with the indicated ligand but without peptide present. <sup>c</sup>Zeta potential of the QD surface functionalized with the indicated ligand. Representative data plots for  $H_{\text{D}}$  and  $\zeta$ -potential can be found in the SI. <sup>d</sup>FRET derived distance from the QD center to the terminal Cy3 dye on the peptide substrate when the QD is capped with the indicated ligand. QD diameter  $\sim 5.4$  nm. Values in parentheses are estimated dye-to-QD surface distances/dye to ligand surface (negative values signify they are found within the estimated diameter of the ligand surface).

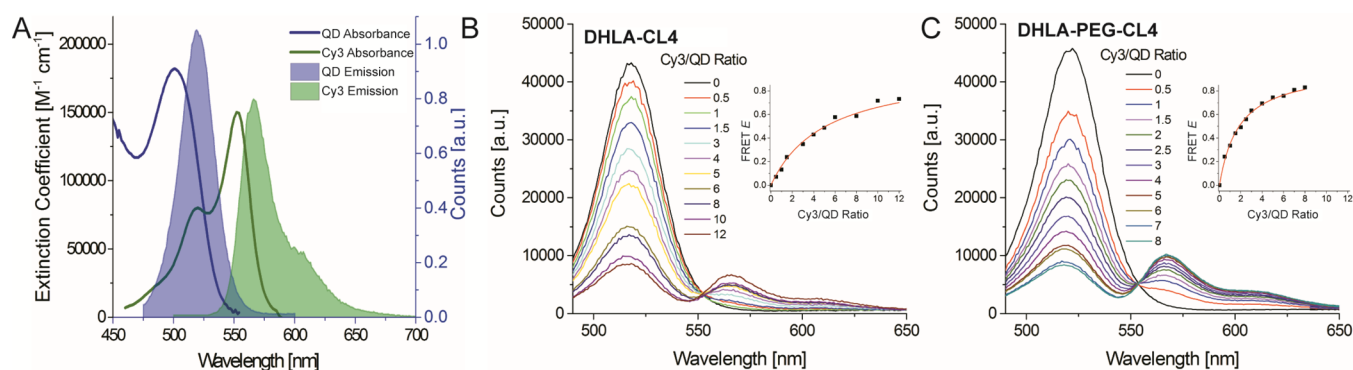


**Figure 2.** Spectral overlap and FRET-based titration of peptide substrates. (A) Extinction coefficient and fluorescence emission spectra of the 520 nm QD donor and Cy3 acceptor. The emission spectra are normalized to quantum yields of 0.20 and 0.17 for the QD and Cy3 respectively. Plot of the spectral profiles collected from the 520 nm QDs surface functionalized with the (B) CL4 and (C) PEG-CL4 ligands and assembled with the indicated number of increasing Cy3-labeled peptide substrates. These plots were collected exciting the QD and then monitoring changes in QD PL and Cy3 acceptor sensitization. The insets show the plots of FRET efficiency ( $E$ ) versus Cy3 peptide/QD ratio which are used to determine the QD-Cy3 donor-acceptor distance ( $r_{DA}$ ).

for the longest  $r_{DA}$  ( $\sim 6.9$  nm) and this is significantly longer than that of QDs functionalized with the PEGylated ligands (5.6–6.2 nm) some of which appear to be within the PEG layer itself. The central portion of this peptide substrate is known to assume a highly bent structure and we have previously shown how conjugation to PEGylated QDs can sometimes induce additional kinks in peptides containing polyproline repeats, which would help explain some of the difference in  $r_{DA}$  values.<sup>19,36</sup> The hydrodynamic diameters ( $H_D$ ) of QDs capped with each of the ligands but without any peptide attached to the surface were also measured by dynamic light scattering (DLS) analysis. As shown in Table 1, the presence of PEG prevails over any small differences from the capping groups giving the PEGylated QDs an average  $H_D$  of  $\sim 11.8 \pm 0.7$  nm (range of 10.9–12.8 nm). In contrast and as expected, the far more compact CL4 molecule provided QDs with a significantly smaller  $H_D$  of  $\sim 8.5 \pm 0.4$  nm. Addition of peptide to the CL4 QDs increased the  $H_D$  showing that the peptide does indeed extend beyond the ligand sphere in this sample and corroborates well with the estimated values described above, see the SI.

**Progress Curves and Kinetic Analyses.** Figure 3 shows experimental results from the QD-COOH ligand construct assembled with an average ratio of 7.9 Cy3-labeled trypsin substrate as a representative example of the data collected and its transformation. Assays used the same batch of commercial trypsin (type I bovine trypsin, Sigma-Aldrich) with the same specific activity of  $\sim 12\,705$  N $_{\alpha}$ -benzoyl-L-arginine ethyl ester (BAEE) units/mg protein as previously to minimize variability and allow us to include that data in the analysis.<sup>19</sup> PL of the QD at 520 nm and sensitized Cy3 at 575 nm were followed over time during assays for each of the indicated concentrations of trypsin shown in Figure 3A,B. These data were then transformed into the Cy3/QD emission ratio and corrected for instrumental drift as shown in Figure 3C. Using the appropriate calibration curve, this data was converted into remaining substrate per QD, Figure 3D, where the much faster activity of the higher enzyme concentrations is clearly observed. In fact, for the three highest trypsin concentrations, the reactions reach completion in only a few minutes. Figure 3E shows a plot of the data as transformed into enzyme time where the data from the wells with less than 168 nM enzyme concentration provide the most information. The higher concentrations provide a few data points in the most important fitting region (from 0 to 400  $\mu$ M s) but principally have

0 remaining substrate values and, although used in the analyses, are not presented here to allow for a more focused image on the area of interest. For the determination with the peptide only control, a dual-labeled peptide was utilized, with the underlying concepts and analysis being similar to that described previously.<sup>19,38</sup>

Overall, we found the most reliable experimental data was obtained when  $\sim 7$ –12 peptide/QD ratios were used as starting points as these have a better signal-to-noise ratio and are within the FRET limits that avoid any internal filter effects.<sup>38</sup> Given this, and the fact that there is some variability in the  $k_{cat}/K_M$  values from QDs assembled with different average ratios of peptide, we utilize  $k_{cat}/K_M$  values from a single average substrate ratio that is close to the above range for the primary comparison. The resulting values are plotted in Figure 3F and listed in Table 2 along with their standard deviations. Values for all other QDs/ratios are in the Table S1, the OME data is from ref 19. The first observation from this comparison was that all the specificity constants are significantly higher as compared to the freely diffusing peptide ( $1.2 \pm 0.2$  mM<sup>-1</sup> s<sup>-1</sup>). In particular, the CL4 ligands impart the largest change with a  $\sim 35$ -fold increase ( $35 \pm 3$  mM<sup>-1</sup> s<sup>-1</sup>) and this is followed by the PEG-CL4 materials with a  $\sim 15$ -fold increase ( $18 \pm 2$  mM<sup>-1</sup> s<sup>-1</sup>). All the other QD constructs result in a 3–12 fold increase in efficiency as compared to the peptide alone. The second observation is a decrease in efficiency as the QD surface goes from negatively charged (CL4, PEG-CL4, COOH, OH) to neutral (OME, COCH<sub>3</sub>) and then an increase as the QD regains a charge, in this case the positive charge of the NH<sub>2</sub>. We note that the  $k_{cat}/K_M$  values for each ligand averaged from all the different peptide ratios in Table S1 also follow the same order of increasing activity and are not significantly different from the representative values in Table 2.

**Molecular Dynamics Simulations.** To corroborate the kinetic data and, more pertinently, gain further insight into the underlying kinetic enhancement mechanism(s), we performed atomistic molecular dynamics (MD) simulations of four representative systems (CL4, PEG-CL4, OMe, and NH<sub>2</sub>) that covered the breadth of observed trypsin activity along with NP surface charge variability and ligand length. The NP models were formed from a 5 nm diameter metallic core with 200 ligands attached homogeneously to the core by the dithiol functionality. The value of 200 was used as it is the midpoint in the previously derived range of 150–250 ligands which was estimated from the

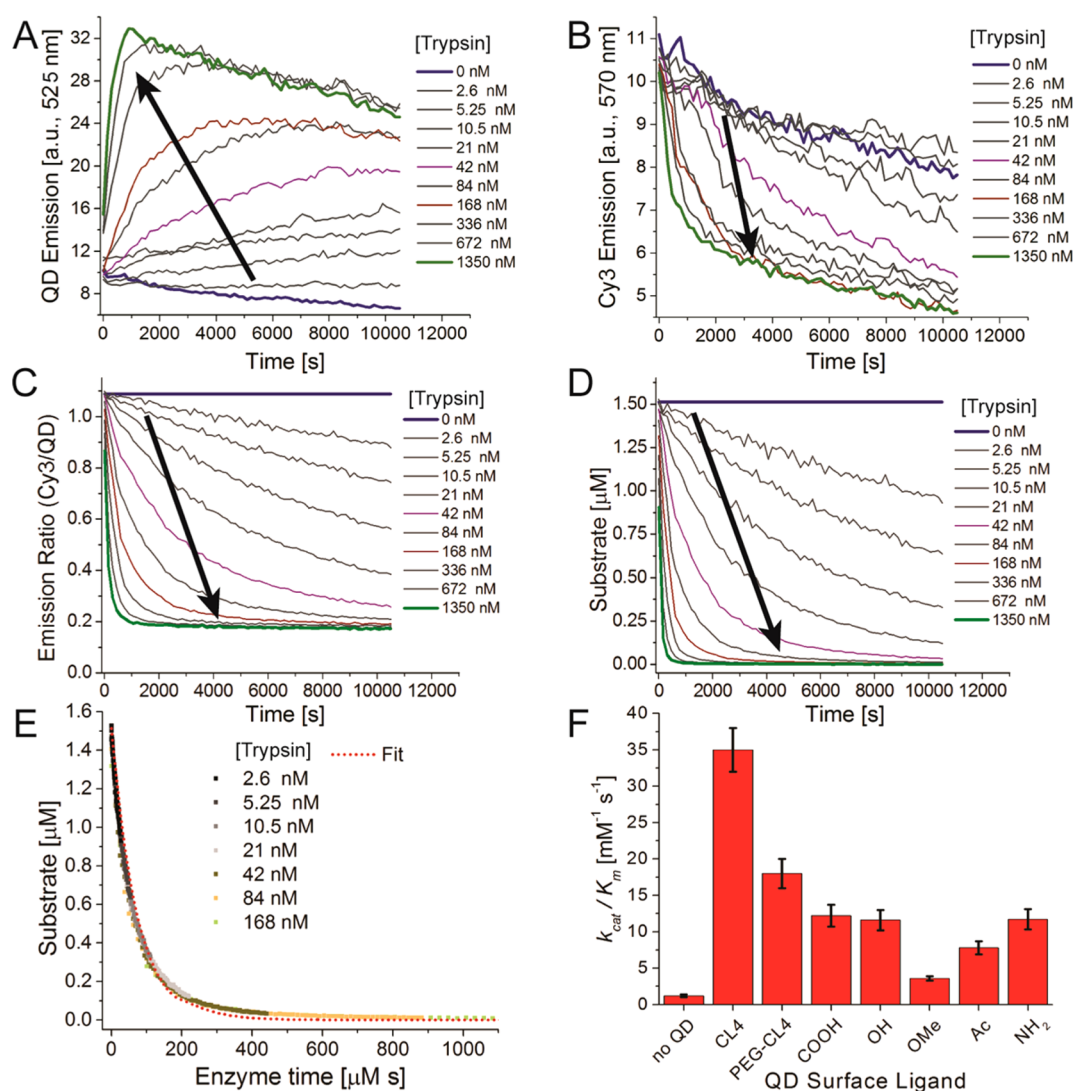


**Figure 3.** Representative kinetic data collected from assaying trypsin activity with COOH-capped QDs assembled with the labeled peptide substrate. Where included, the black arrows denote increasing enzyme concentration. (A) 520 nm QD donor and (B) Cy3 acceptor PL as a function of time when exposed to the indicated increasing concentrations of trypsin. An average ratio of 7.9 Cy3-labeled peptides were assembled on the QDs for these experiments. (C) Cy3/QD emission ratio as a function of time. The data has been corrected for the experimental drift seen in panels A, B. (D) Remaining intact substrate per QD as a function of time. The data in part C is converted to these values based on the corresponding calibration curves. (E) Data set shown in D transformed into enzyme time ( $[\text{Trypsin}] \times \text{time}$ ) progress curves. The red-dotted line represents the fit to the data that allows for retrieval of the enzyme efficiency ( $k_{\text{cat}}/K_M$ ) values. (F) Averaged  $k_{\text{cat}}/K_M$  values for the peptide control with no QD present and with OMe functionalized QDs (from ref 19) as compared to QD-peptide assemblies displaying each of the current surface ligands.

**Table 2. Trypsin Enzymatic Efficiency of Selected QD-Peptide Substrates Displaying Different Surface Ligands**

surface ligand	peptide/QD ratio	$k_{\text{cat}}/K_M$ [ $\text{mM}^{-1} \text{s}^{-1}$ ]
Peptide only (no QD)	—	$1.2 \pm 0.2^a$
CL4	7.0	$35 \pm 3$
PEG-CL4	8.1	$18 \pm 2$
COOH	7.9	$12.2 \pm 1.5$
OH	8.0	$11.6 \pm 1.4$
OMe	7.0	$3.6 \pm 0.3^a$
Ac	5	$7.8 \pm 0.9$
$\text{NH}_2$	8.2	$11.7 \pm 1.4$

<sup>a</sup>Value from ref 19. See Table S1 for other peptide/QD ratio values.

fitting maxima for DHLA ligands on a ZnS coated QD of similar size (diameter  $\sim 5.8$  nm).<sup>50</sup> This range was arrived at by

considering the 2 different conformations that DHLA may assume on the surface of a QD with either a flat-folded or linearly extended conformation.<sup>50</sup> These simulations were geared toward providing insight into 2 critical aspects of how trypsin interacted with these QD-ligand-peptide assemblies, namely, (i) the behavior of peptides as displayed around the nanocrystals functionalized with different ligands, and (ii) the interaction of trypsin with the NP surface. The systems were simulated in a 150 mM physiological NaCl solution pH 7.4, see the Methods for more details.<sup>51</sup>

In the first study, four peptide molecules were attached to the NP core through their terminal hexahistidine residue to simulate their behavior since peptide exposure and cleavage site availability/accessibility should correlate with increased proteolysis. The representative image captures shown in Figure 4A suggest that during the 80–90 ns simulations the peptides on the OMe,  $\text{NH}_2$  and PEG-CL4 QD materials are to a large extent

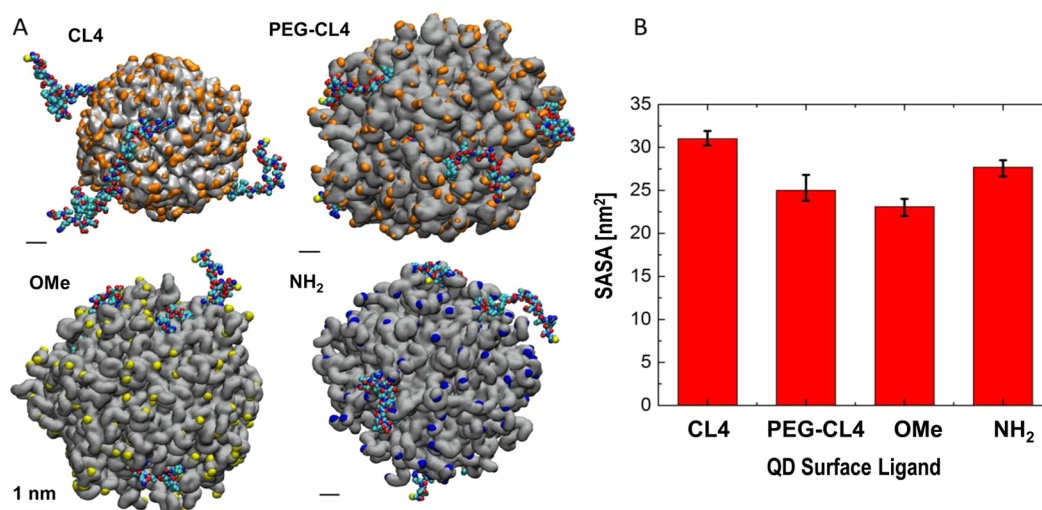


**Figure 4.** Simulated display of the Cy3-labeled peptide substrate on the surface of the QDs. (A) Energy-minimized simulations highlighting peptide configurations on the surface of the CL4, PEG-CL4, OMe and NH<sub>2</sub> ligand functionalized QDs. Orange designates the NH<sub>3</sub><sup>+</sup> and COO<sup>-</sup> groups in the CL4 and PEG-CL4 ligand simulations while yellow represents the OMe group on the OMe ligand and blue shows the NH<sub>3</sub><sup>+</sup> in the NH<sub>2</sub> system. The heavy atoms of the peptide are shown by a van der Waals representation. Scale bars are 1 nm. (B) Estimated solvent accessible surface area (SASA in nm<sup>2</sup>) reflecting the water exposed surface area of the peptide when assembled on the indicated QDs.

intertwined in the ligand corona with only their termini extending out from this field. In direct contrast to this observation, a significantly greater portion of the peptide appears to be clearly extended out from the QD functionalized with the smaller zwitterionic CL4 ligand. To provide a somewhat more quantitative metric to this behavior, we calculated the solvent accessible surface area (SASA) of the whole peptide for each of the ligand simulations with water as the solvent, see Figure 4B. To accomplish this, the average peptide SASA for each configuration over the last 100 frames (1 ns) of the simulation was collected. The peptides have the smallest amount of exposure in the OMe ligand system and the largest amount in the CL4 system with about 35% more relative SASA. We note that the ascending order of peptide exposure is OMe (~23.1 nm<sup>2</sup>) < PEG-CL4 (~25 nm<sup>2</sup>) < NH<sub>2</sub> (~27.7 nm<sup>2</sup>) < CL4 (~31 nm<sup>2</sup>) and this correlates reasonably well with the ascending order of increasing enzyme efficiency or  $k_{\text{cat}}/K_{\text{M}}$  value observed above: OMe < NH<sub>2</sub> < PEG-CL4 < CL4 (Table 2).

Clearly, there is some correlation between the SASA values and the observed efficiencies. At a first pass, this may be primarily explainable by the length of the ligand molecules in combination with the chemical nature of the terminal functional groups. The PEGylated OMe ligand is the largest of all the capping moieties used here and has ~16 repeated ethylene oxide units in its PEG module as compared to the ~13 found in the others. Ligand size and chain length are all significantly reduced in the minimal CL4 molecule. The exposure of the peptide in the NH<sub>2</sub> system is also 11% higher than that of the PEG-CL4 and is further 20% more than that of the larger OMe ligands. In this case, electrostatic repulsion between the NH<sub>2</sub> ligand's terminal amine and the amines found on the peptide, including especially the N-terminus and Arg residue, may contribute to more solvent accessibility. However, as discussed below, the positive ligand surface can also attract negative charges on the peptide making this interpretation far more complex and nuanced than this simple interpretation.

In the second study, we simulated QDs in the presence of (four) different trypsin orientations as the trypsin interacted with the surface without the conjugated peptides present. This was undertaken so as to provide information on how trypsin would

interact with a given NP surface as this could also significantly influence peptide cleavage rate. Using a water dielectric constant of 78.5, the electrostatic and van der Waals (vdW) coupling strength of the enzymes to each surface were estimated from the last 0.5 ns of the simulations. Figure 5A shows enzyme configurations on the NP surface which have the strongest observed interactions as listed in Figure 5B. The enzyme-NP coupling strength visibly depends on the surface ligand type and this appears to be clearly influenced by trypsin's net positive charge at pH = 7.4 which is predicted to be +5. For example, in the OMe system, the surface is essentially neutral, giving almost zero electrostatic enzyme-NP coupling, but yet retains quite a large predicted vdW attraction of ~ -70.0 kcal/mol. For the negatively charged PEG-CL4 and CL4 ligand systems, the predicted Coulombic force is ~ -13.0 kcal/mol and ~ -28.0 kcal/mol, respectively. The large electrostatic coupling of CL4 can potentially be explained by multiple (concerted) interactions of short ligands.<sup>25</sup> The longer PEG-CL4, however, provides a vdW coupling of ~ -90.0 kcal/mol while the CL4 predicts a value of ~ -15.0 kcal/mol. For the positively charged NH<sub>2</sub> system, the enzyme should be adsorbed on the surface, due to a vdW coupling of ~ -30.0 kcal/mol, but this adsorption may not be very stable due to potentially repulsive electrostatic coupling with an estimated value of ~9.0 kcal/mol. Alternatively, the positively charged NH<sub>2</sub> surface may also potentially attract negative amino acid charges on the surface of the enzyme which could constrain it in energetically favorable orientations, but which may be sterically unfavorable for peptide-enzyme interactions. Such coupling-favored orientations have been suggested before for similarly functional proteases acting on QD-peptides substrates and could certainly act to inhibit enhanced enzymatic activity in this case.<sup>52</sup> When the overall electrostatics are not favorable, the NP-enzyme interaction will tend toward a short lifetime due to weak attractive vdW interactions. Overall, the obtained interaction profiles in Figure 4B (PEG-CL4 > OMe > CL4 > NH<sub>2</sub>) do not corroborate with the observed experimental data. This suggests that, although they may certainly contribute to associating trypsin with the QD surface and increasing time

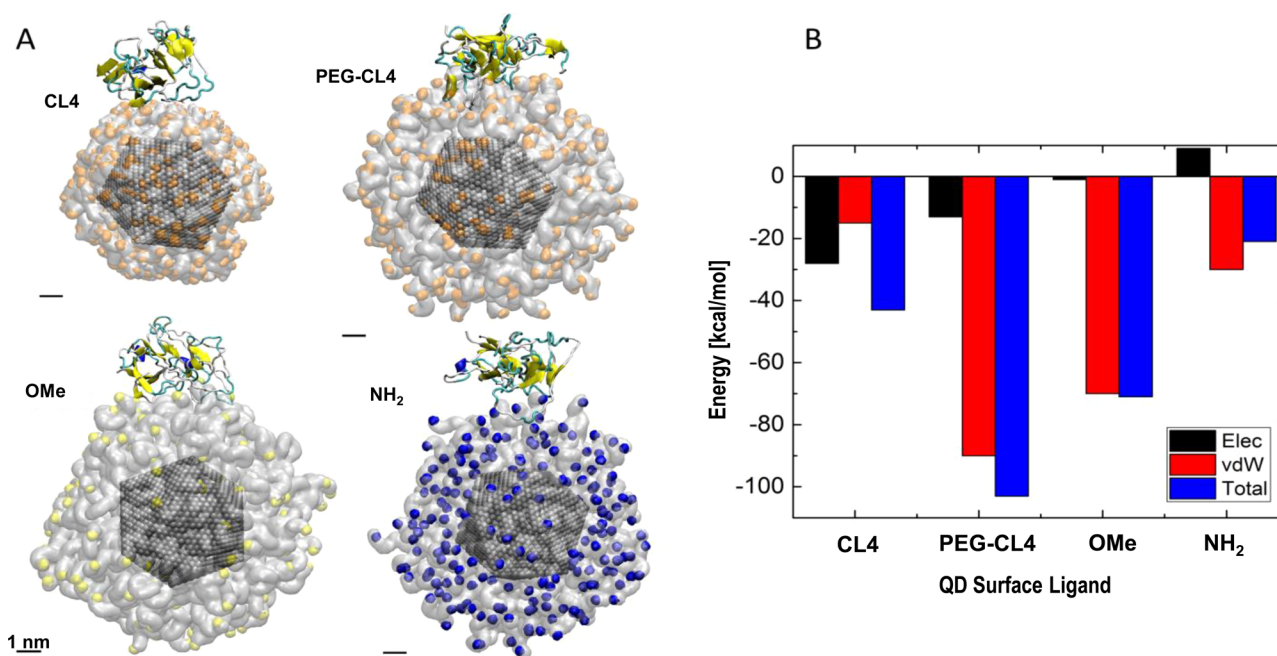


**Figure 5.** Adsorption of trypsin to the different QD surfaces. (A) Trypsin enzymes are shown in cartoon representation as ball and ribbon. Configurations where the enzyme has the strongest interaction with NP surfaces are shown in cartoon representations. (B) Electrostatic (Elec), van der Waals (vdW), and total coupling strength estimated between the trypsin and the QD surfaces.

spent localized on the QD, they are not, in and of themselves, the sole source of enhancement.

Monitoring trypsin activity on QD-peptide substrates functionalized with different surface ligands clearly reveals significant increases in enzyme efficiency depending upon the ligand chemistry present. In comparison to the 5-fold improvements over freely diffusing trypsin-peptide formats we noted previously for the OMe QDs,<sup>19</sup> use of CL4 ligands now provide for ~35-fold improvements in efficiency. This is actually a conservative estimate as the highest efficiency we observed with that ligand was ~60-fold and the average efficiency over all peptide ratios with that QD material was  $45 \pm 14 \text{ mM}^{-1} \text{ s}^{-1}$ , see Table S1. We utilize the lower value in Table 2 to be conservative and not overly bias the results. Cumulatively, this data strongly supports our initial conjecture that the NP surface ligands can have a dominating influence over enzyme activity at the nanoscale interface, at least for this configuration. Atomistic MD simulations were utilized to help understand two key components/interactions of this system: (i) peptide conformation when assembled to QDs with four different representative ligands, and (ii) trypsin interactions with the same ligands as displayed around the QD. Analyzing the trypsin activity profiles for each ligand configuration in combination with results from the simulations and a current understanding of how trypsin interacts with a substrate and catalyzes a proteolytic event helps provide strong insight into the mechanisms that underpin how activity is enhanced for this materials configuration.

The MD simulations confirmed that one important characteristic to be considered when describing these type of NP displayed peptide substrate-enzyme interactions is that of cleavage site availability. The activity profiles suggest that there is almost a bimodal distribution of enzyme efficiency that can be roughly grouped as CL4 > the remaining ligands, see Table 2. Assemblies based on the CL4 ligand are the most efficient ( $\sim 35 \text{ mM}^{-1} \text{ s}^{-1}$ ) with the rest of the ligands displaying a range of efficiencies

starting at around half this value ( $\sim 18 \text{ mM}^{-1} \text{ s}^{-1}$  for PEG-CL4 ratio = 8.1) and then decreasing down to values associated with the OMe ligand which is *ca.* 3–5 $\times$  smaller ( $\sim 4 \text{ mM}^{-1} \text{ s}^{-1}$ ). Nanocrystals capped with CL4 also provide for the largest QD donor-Cy3 acceptor  $r_{\text{DA}}$  of almost 7 nm, have the most negative  $\xi$ -potential ( $-32.4 \text{ mV}$ ), the smallest  $H_{\text{D}}$ , and the largest SASA value (see Table 1, Figure 4). The effect of all this is more definitively shown in Figure 4A where the peptide substrate has the most extension away from the smaller ligand shell and, by default, the most availability for enzyme binding/cleavage. The fact that the PEG-CL4 QDs show the second highest efficiency is also important as it suggests either a strong role for the zwitterionic end group in the kinetic enhancement or the contribution of strong attractive coupling or even both. We note that the  $H_{\text{D}}$  value for the NH<sub>2</sub> ligand is the second smallest after the CL4 materials while its  $r_{\text{DA}}$  is comparable to the other QDs. The simulation and SASA results in Figure 4 also suggest some peptide accessibility but this is not as profound as that seen for the CL4. The only other major difference is the  $\xi$ -potential which, at 21.3 mV, is strongly positively charged. The efficiency of the NH<sub>2</sub> ligand is, however, comparable to that of the COOH and OH systems which are more negatively charged.

Examining the second characteristic of interest, namely the attraction between the enzyme and the surface ligands, shows this to be more complex and not so definitive. Assuming the trypsin to be slightly positively charged (*ca.* +5) and looking to the  $\xi$ -potentials (Table 1) shows the most negative materials to be the CL4, PEG-CL4 and COOH capped QDs where the first 2 also produce the highest efficiencies. However, Figure 5b reveals that the vdW coupling strength is in fact far larger than the electrostatics and does not correlate to the efficiency trends. For example, the poorest performing OMe system has almost no electrostatic component and a vdW of  $-70 \text{ kcal/mol}$ ; this is much larger in comparison to the CL4 electrostatic and vdW combined ( $-43 \text{ kcal/mol}$ ) but not as large as the PEG-CL4



which is  $-100$  kcal/mol. Looking just at these coupling strengths would suggest the PEG-CL4 and OMe should have higher efficiencies than CL4 which is not the case. Interestingly, the OMe vdW component may, in part, explain the capability of some of the neutral systems to show greater enzymatic efficiency than the freely diffusing peptide as they may help increase the enzymes residence time on the QD surface. Overall, what becomes apparent is that both variables (exposure of the peptide and the coupling of the enzyme on the NP surface) must work in concert. For example, the OMe had the second highest attractive nature for trypsin, in fact  $>2$ -fold that of the  $\text{NH}_2$ , yet the  $\text{NH}_2$  has a greater  $k_{\text{cat}}/K_{\text{M}}$  as the peptide availability here was 20% higher. This concept is epitomized by comparing the CL4 (greater peptide availability) and PEG-CL4 (greater trypsin attraction) results. This suggests why the latter has the second highest efficiency after CL4 even while having significantly less peptide availability. This trend is then reversed for PEG-CL4 in comparison to the  $\text{NH}_2$ , where the former has a greater efficiency even with a lower SASA value. Here, we suggest that the greater coupling strength is more dominant. Increased coupling strength can help place the trypsin on the QD surface and increase its residence time there. What we cannot infer from these simulations is if the combined coupling or attractive force also contributes to the trypsin having a “productive” orientation, *i.e.*, binding site available relative to the peptide substrate orientation, as it interacts with the QD.

Beyond this, we suggest that there are other factors that may also contribute to improvements or decreased efficiency for a given ligand and these are more inferred from the simulation data. They are associated with trypsin’s structure itself and how it interacts with substrate and the nature of how it chemically cleaves a peptide substrate. Trypsin’s catalytic site is located in a relatively large-deep binding pocket or cleft and so this will require a lot of the peptide substrate to be available with unhindered access for a productive interaction to occur. As shown in the comparative schematics in Figure 6, here is where the small size of the CL4 ligand makes a definitive difference. It allows trypsin easy access to the region of the peptide substrate to be cleaved and this is paired with an easy fitting of this region within the enzymes deep binding cleft (Figure 6A). The enzyme radius is  $\sim 1.5$  nm,<sup>53</sup> meaning that it “fits” relatively well between the CL4 surface and the cleavage site ( $\sim 2.6$  nm, assuming a rigid CL4 ligand layer).

The bulkier PEG groups present on all the other ligands add  $\sim 2$  nm of additional polymer surface. This could serve to decrease productive interactions to some extent as they will be far less frequent along with perhaps preventing the enzyme from attaining the deep penetration of the peptide into the cleft that is needed for proteolysis (Figure 6B). This effect is again epitomized by comparing the results of the CL4 system *versus* that of the PEG-CL4 system where the ligand’s end groups are the same and the only difference is the presence of the latter’s PEG group (Table 2, Figure 5). As discussed above, based on trypsin-ligand coupling strength alone the latter should be far more efficient.

Trypsin contains a catalytic triad of amino acids which stabilize the oxyanion hole through electrostatic charges therefore increasing the nucleophilicity of the active site pocket.<sup>54</sup> Shifts in the charge of the enzyme and substrate nanoenvironment, something that may be expected with changes in the QD ligand choice, may therefore result in modified kinetics.<sup>55</sup> The  $\text{pK}_{\text{a}}$  of trypsin’s active site is crucial to enzyme activity and it is further believed that changes to the  $\text{pK}_{\text{a}}$  of sites far from the catalytic site may also play a contributing role.<sup>55,56</sup> Research into trypsin activation has also shown that modification of the availability and structure of water molecules in the environment of trypsin or substrate may also modify the kinetics.<sup>54,56</sup> Related to this, the fact that both the positively charged and negatively charged QD surface increased the  $k_{\text{cat}}/K_{\text{M}}$  of the enzyme, which is positively charged at the chosen pH, appeared surprising. Some mechanistic evidence was provided by the MD simulation, but the level of enhancement as compared to the Ac and OMe ligands was still unforeseen. This effect might be understood by taking a closer look at the energetics of trypsin catalysis. The reaction proceeds through the formation of a negatively charged intermediate that acts as a nucleophile on the peptide bond. As stated by Warshel and Russell “the stabilization of the intermediate’s oxyanion hole by internal water molecules, contributing up to 40 kcal/mol, is the most important catalytic factor”.<sup>54</sup> Specifically the peptide- $\text{H}_2\text{O}$  structure in the vicinity of Ser-195 is crucial. This correlates clearly with the trend observed in the QD-ligand choice. The inclusion of a PEG section not only sterically hinders the approach of the enzymes active site, but it may also greatly reduce the local prevalence of water in the peptide vicinity.<sup>57</sup> Even within the PEGylated ligand choices the more hydrophobic

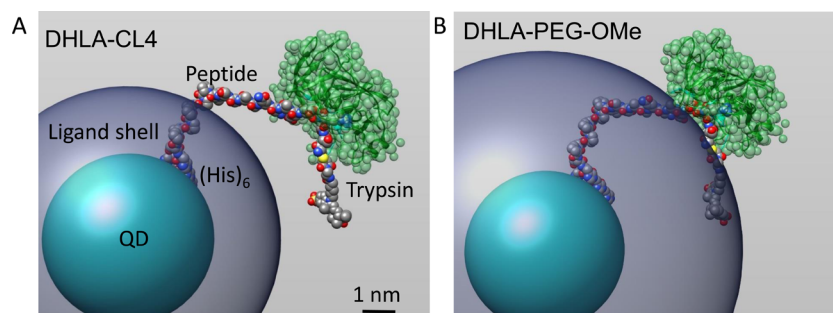


**Figure 6.** Models of trypsin binding to the peptide substrate when the QDs are functionalized with different surface ligands. Models of the (A) CL4-functionalized QDs and (B) OMe-functionalized QDs were simulated as in ref 19 with some modifications. The core/shell structure of the QD is simulated by the aqua central sphere with a diameter of 5.6 nm which is slightly larger than the experimentally used QDs; the increased size is used for visualization. The surrounding ligands are simulated by the dark blue sphere where the length was adjusted to match those seen in Figure 4. The peptides are shown in a space-filling mode with all of the  $(\text{His})_6$  interacting with the QD surface. The location of the peptide termini were adjusted to match the QD donor-dye acceptor separation distances estimated by FRET analysis (Table 1). Trypsin is shown with the space-filling atoms in translucent green surrounding the ribbon structure and is bound to the peptide with its arginine and surrounding residues positioned in the cleavage site. These are only simulations and represent one of many peptide and enzyme conformations that are possible.

(less charged) capping heads correlate somewhat with reduced  $k_{\text{cat}}/K_M$ . Supporting this notion, there is mounting evidence that the interfacial environment found at the NP surface is considerably different from that of bulk solution and that the water present here may actually be structured.<sup>23,24</sup> Some of the other physicochemical changes that are postulated to occur here include charge and ionic gradients along with altered  $\text{p}K_a$ 's, boundary layers and phase separation along with alterations to density, solvation, viscosity and the like. However, there is still not enough of an understanding of this environment to predict such changes nor do any analytical techniques yet exist for robustly probing them.<sup>58</sup> Nevertheless, based on this we can still postulate that modification(s) to the electrostatics and  $\text{p}K_a$ 's of trypsin's amino acids originating from the different capping ligand surfaces and nanoenvironment around the QDs may also influence enzyme activity.

## CONCLUSIONS

Overall, we find through both experiments and simulation that a complex set of factors influence trypsin's activity on QD-peptide substrates and that the nature of the surface ligand is critical to this. We find peptide substrate availability and enzyme binding site accessibility to that peptide substrate as displayed on the QD to be the most significant factor for enhanced activity although attractive forces and coupling strength probably also contribute to a large extent. The latter would help place the trypsin on the QD surface and increase its residence time there. This exercise also strongly suggests that applying a similar methodology to other NP-enzyme systems can certainly help understand how they function and provide valuable insight in order to improve their design and activity. Coming full circle back to the potential of bionanotechnology and specific application areas such as therapeutics, the cumulative knowledge gained from multiple such studies can certainly help contribute to the next generation of highly efficient bionano composite materials.

## METHODS

**Materials.** CdSe/ZnS core/shell QD with an emission maxima centered at  $\sim 520$  nm (diameter  $5.3 \pm 0.6$  nm, see the SI for TEMs) were synthesized as described.<sup>43</sup> A complete description of the chemical syntheses used to prepare the QD surface ligands in this study is provided in the SI. QDs were cap exchanged with the selected ligands and dispersed in aqueous medium as described.<sup>43,45</sup> The trypsin peptide substrate  $N$ -\*CSTRIDEANQAATSLP;SH<sub>6</sub>-COOH was obtained from Biosynthesis (Lewisville, TX) and labeled with a Cy3 maleimide (GE healthcare, PA13131) on the cysteine thiol\*, purified, desalted, lyophilized and stored frozen until use as previously described.<sup>19,59</sup> Trypsin was purchased from Sigma-Aldrich (Type I bovine trypsin, T1005) as a lyophilized powder and dissolved in buffer immediately prior to use. Samples were assayed in 1× phosphate buffered saline (PBS: 137 mM NaCl, 10 mM phosphate, 2.7 mM KCl, pH 7.4). 0.2  $\mu\text{m}$  poly(ether sulfone) membrane sterile syringe filters were from VWR.  $\text{p}K_a$  values for selected ligands were calculated using ACD/PhysChem Suite version 12.01 by Advanced Chemistry Development, Inc., Toronto, ON, Canada.

**QD-Peptide Self Assembly.** Stock solutions of QDs with the selected surface ligands were diluted into 1× PBS buffer and the Cy3-labeled peptide, also dissolved in PBS, was added to the QDs in the desired substrate to QD ratio.<sup>19,59</sup> Self-assembly of the peptides to the QD surface was allowed to proceed for at least 30 min to 1 h prior to being diluted for any subsequent measurements or analysis.

**Characterization.** Absorbance spectra were obtained on an Agilent 8453 UV-visible Chemstation with 1× PBS solution as a blank. Fluorescence spectra utilized for the calibration curves were obtained on a Tecan Infinite M1000 Dual Monochromator Multifunction Microtiter

Plate Reader (Tecan, Research Triangle Park, USA) utilizing microtiter 96-well plates (100  $\mu\text{L}$  per well). Excitation was at 400 nm with 1 nm emission steps from 450 to 700 nm with an integration time of 20  $\mu\text{s}$ . Details on fluorescence measurements in the kinetic assays are provided below. Dynamic light scattering (DLS) analysis was measured on a Nano-ZS Zetasizer Nanoseries (Malvern Instruments) as described.<sup>43,45,60</sup> Before measurements, QD peptide assemblies were prefiltered through 0.2  $\mu\text{m}$  syringe filters to remove impurities in the sample. Measurements were taken at 20 °C and each sample underwent an average of three runs of 10 s each.  $\zeta$ -potential was also measured on the Nano-ZS Zetasizer Nanoseries. Solutions were filtered with 0.2  $\mu\text{m}$  filters and dilutions made with 0.1× PBS. Transmission electron microscopy (TEM) was carried out on the QDs using a JEOL 2200-FX analytical high-resolution transmission electron microscope at 200 kV accelerating voltage on an ultrathin carbon/holey support film on a 300 mesh Au grid (Ted Pella, Inc.).

**Trypsin Proteolytic Assays.** For assembling the initial calibration curves prior to each experiment, an increasing ratio of QD-(peptide-Cy3)<sub>*m*</sub> conjugates (with *m* typically in the range of 0–15 using increments of 2 or 3) were self-assembled by mixing QDs (20 pmol; 0.2  $\mu\text{M}$ ) with the Cy3-labeled peptide in PBS for 30 min to 1 h. Full spectra along with Cy3 acceptor ( $\sim 575$  nm) and QD donor ( $\sim 520$  nm) PL maxima values were then collected on a Tecan Infinite M1000 Fluorescent Microtiterwell Plate Reader. QD assemblies with varying surface ligands were then prepared at the desired substrate to QD ratio at a final QD concentration of 0.4  $\mu\text{M}$  before the addition of the enzyme. A series of trypsin dilutions (50  $\mu\text{L}$  at 0, 2.6, 5.25, 10.5, 21, 42, 84, 168, 336, 672, 1350 nM) were loaded in sequential wells of a Corning Costar Flat Black 96 well microtiter plate in duplicate rows. Utilizing an automated pipetter, 50  $\mu\text{L}$  of the QD-sensor was quickly added to each enzyme well and the kinetic measurement program on the Tecan Infinite M1000 Plate Reader was started immediately after the final addition. Using an excitation wavelength of 400 nm, Cy3 acceptor ( $\sim 575$  nm) and QD donor ( $\sim 520$  nm) PL maxima were collected from each well every 150 s while maintaining the plate temperature at 25 °C for a minimum of 2 h. Assay plates underwent 3–5 s of orbital shaking after each reading. Progress curves were derived from this raw data as described.<sup>19,21,61</sup>

**Förster Resonance Energy Transfer Analysis.** QD donor center to Cy3 acceptor dye separation distances were estimated from the FRET data as described.<sup>62,63</sup> A system consisting of a spherical centrosymmetric single QD donor surrounded by multiple acceptor-dye labeled peptides with a single Förster distance ( $R_0$ , 5.25 nm) and an average QD donor-dye acceptor separation ( $r_{\text{DA}}$ ) was assumed for the sensor assemblies. In these constructs, a single QD-donor will transfer energy to one of the multiple Cy3 acceptors through FRET. The FRET efficiency for a single donor-multiple acceptor system ( $E_n$ ) can be calculated with<sup>62,63</sup>

$$E_n = \frac{N \left( \frac{R_0}{r_{\text{DA}}} \right)^6}{1 + N \left( \frac{R_0}{r_{\text{DA}}} \right)^6} \quad (1)$$

where  $N$  is the number of acceptors per QD. It is generally accepted that, with the spherical symmetry of the QD, the dyes are equivalent with  $r_{\text{DA}}$  representing the distance distribution of the  $N$  dye acceptors to the center of the QD, though the different surface ligands will result in varying  $r_{\text{DA}}$  values. With proper calibration curves, changes to the donor-acceptor ratiometric signal, which is a readout of the FRET  $E$  during an assay, can be correlated to the amount of uncleaved peptide remaining bound to the QD.<sup>38</sup> It is important to note that the different proteolysis models (Hopping and MM) still result in similar FRET progress curves in ensemble measurements.<sup>20</sup> The  $R_0$  in eq 1 was estimated with eq 2:

$$R_0^6 = C_0 \kappa^2 J n^{-4} Q_D \quad (2)$$

where  $C_0$  is a constant ( $8.8 \times 10^{-28}$  if  $R_0$  is expressed in nm),  $\kappa^2$  is the dipole-dipole orientation factor assumed to be 2/3,<sup>62,64</sup>  $J$  is the spectral overlap of the donor emission and the acceptor absorption

( $5.3 \times 10^{15} \text{ nm}^4 \text{ M}^{-1} \text{ cm}^{-1}$ ),  $n$  is the average refractive index (using the value of water 1.33), and  $Q_D$  is the donor quantum yield in the absence of the acceptor which was measured at 0.2.

**Enzymatic Kinetic Analysis.** Raw emission-ratio progress curves were transformed into peptide/QD ratios by utilizing calibration curves to determine the peptide/QD ratios and the known quantities of QD concentration as described.<sup>19,21,38</sup> The curves were corrected for instrumental drift by using a control data series with no enzyme added. Corrected data was converted into a progress curve of remaining substrate as a function of time. By multiplying the reaction time (in seconds) by the enzyme concentration (in mM) for each measurement the data is converted into the enzyme-time progress curves (X-axis) while the Y-axis continues to be remaining substrate, for example, see Figure 3. Data were analyzed using the time-integrated version of the Michaelis–Menten (MM) equation:

$$k_{\text{cat}} \times Et = p + K_M \times \ln\left(\frac{a_0}{a_0 - p}\right) \quad (3)$$

where  $k_{\text{cat}}$  is the catalytic rate,  $E$  is enzyme,  $t$  is time,  $p$  is the reaction product concentration,  $K_M$  is the Michaelis constant which reflects enzyme affinity for substrate, and  $a_0$  is the initial substrate concentration. Nonlinear regression fitting of the progress curves were realized using an in-house developed Wolfram Mathematica 10.0 Notebook with the result being estimates of the  $k_{\text{cat}}/K_M$  ratios.

**Molecular Dynamics Computational Analysis.** The trypsin structural coordinates utilized was 2PTN from the Protein Data Bank ([www.rcsb.org](http://www.rcsb.org)).<sup>65</sup> Ligands were assembled from the individual chemical structures and arrayed around an assumed NP of diameter 5 nm. All MD simulations were performed in a 150 mM physiological salt solution with a pH of 7.4 and ligand  $pK_a$ 's were utilized where available. Chemistry at Harvard Macromolecular Mechanics (CHARMM) general and protein force field were used to model the systems.<sup>66–69</sup> In simulations, nonbonding interactions were calculated using a cutoff distance of  $d = 10 \text{ \AA}$  and long-range electrostatic interactions were calculated by the Particle Mesh Ewald (PME) method in the presence of the periodic boundary conditions.<sup>70</sup> We simulated the systems in a fixed number of atoms constant-temperature, constant-pressure (NPT) ensemble using Langevin dynamics with a damping coefficient of  $\gamma_{\text{Lang}} = 0.1 \text{ ps}^{-1}$  and a time step of 2 fs. All systems were simulated with Nanoscale Molecular Dynamics (NAMD) for 80–90 ns or longer.<sup>51</sup>

## ASSOCIATED CONTENT

### Supporting Information

The Supporting Information is available free of charge on the ACS Publications website at DOI: 10.1021/acsnano.7b01624.

Details of ligand syntheses, TEM, and selected data on the QD-ligand systems and their assay performance (PDF)

## AUTHOR INFORMATION

### Corresponding Authors

\*E-mail: [pkral@uic.edu](mailto:pkral@uic.edu).

\*E-mail: [igor.medintz@nrl.navy.mil](mailto:igor.medintz@nrl.navy.mil).

### ORCID

Sebastián A. Díaz: 0000-0002-5568-0512

Petr Král: 0000-0003-2992-9027

Igor L. Medintz: 0000-0002-8902-4687

### Author Contributions

▲S.A.D. and S.S. contributed equally.

### Notes

The authors declare no competing financial interest.

## ACKNOWLEDGMENTS

I.L.M. acknowledges the NRL NSI and USDA grant No. 2016-67021-25038. P.K. was supported by the NSF DMR grant No.

1309765. S.A.D. acknowledges an ASEE Fellowship through NRL. The authors thank Advanced Chemistry Development, Inc., Toronto, ON, Canada for assistance with analyzing ligand  $pK_a$  values.

## REFERENCES

- (1) Krishnan, U. M.; Sethuraman, S. The Integration of Nanotechnology and Biology for Cell Engineering: Promises and Challenges. *Nanomater. Nanotechnol.* **2013**, *3*, 19.
- (2) Parandian, A.; Rip, A.; Te Kulve, H. Dual Dynamics of Promises, and Waiting Games around Emerging Nanotechnologies. *Technology Analysis & Strategic Management* **2012**, *24*, 565–582.
- (3) Reddy, K. G.; Deepak, T. G.; Anjusree, G. S.; Thomas, S.; Vadukumpully, S.; Subramanian, K. R. V.; Nair, S. V.; Nair, A. S. On Global Energy Scenario, Dye-Sensitized Solar Cells and the Promise of Nanotechnology. *Phys. Chem. Chem. Phys.* **2014**, *16*, 6838–6858.
- (4) Medintz, I. Universal Tools for Biomolecular Attachment to Surfaces. *Nat. Mater.* **2006**, *5*, 842.
- (5) Samanta, A.; Medintz, I. L. Nanoparticles and DNA—a Powerful and Growing Functional Combination in Bionanotechnology. *Nanoscale* **2016**, *8*, 9037–9095.
- (6) Boisselier, E.; Astruc, D. Gold Nanoparticles in Nanomedicine: Preparations, Imaging, Diagnostics, Therapies and Toxicity. *Chem. Soc. Rev.* **2009**, *38*, 1759–1782.
- (7) Sapsford, K. E.; Algar, W. R.; Berti, L.; Gemmill, K. B.; Casey, B. J.; Oh, E.; Stewart, M. H.; Medintz, I. L. Functionalizing Nanoparticles with Biological Molecules: Developing Chemistries That Facilitate Nanotechnology. *Chem. Rev.* **2013**, *113*, 1904–2074.
- (8) Escudero, A.; Carrillo-Carrion, C.; Zyuzin, M. V.; Parak, W. J. Luminescent Rare-Earth-Based Nanoparticles: A Summarized Overview of Their Synthesis, Functionalization, and Applications. *Top. Curr. Chem.* **2016**, *374*, article # 48.
- (9) Wen, A. M.; Steinmetz, N. F. Design of Virus-Based Nanomaterials for Medicine, Biotechnology, and Energy. *Chem. Soc. Rev.* **2016**, *45*, 4074–4126.
- (10) Banholzer, M. J.; Millstone, J. E.; Qin, L. D.; Mirkin, C. A. Rationally Designed Nanostructures for Surface-Enhanced Raman Spectroscopy. *Chem. Soc. Rev.* **2008**, *37*, 885–897.
- (11) Dykman, L. A.; Khlebtsov, N. G. Multifunctional Gold-Based Nanocomposites for Theranostics. *Biomaterials* **2016**, *108*, 13–34.
- (12) Kilcoyne, A.; Harisinghani, M. G.; Mahmood, U. Prostate Cancer Imaging and Therapy: Potential Role of Nanoparticles. *J. Nucl. Med.* **2016**, *57*, 105S–110S.
- (13) Ling, D. S.; Hackett, M. J.; Hyeon, T. Surface Ligands in Synthesis, Modification, Assembly and Biomedical Applications of Nanoparticles. *Nano Today* **2014**, *9*, 457–477.
- (14) Othman, A.; Karimi, A.; Andreescu, S. Functional Nanostructures for Enzyme Based Biosensors: Properties, Fabrication and Applications. *J. Mater. Chem. B* **2016**, *4*, 7178–7203.
- (15) Johnson, B. J.; Russ Algar, W.; Malanoski, A. P.; Ancona, M. G.; Medintz, I. L. Understanding Enzymatic Acceleration at Nanoparticle Interfaces: Approaches and Challenges. *Nano Today* **2014**, *9*, 102–131.
- (16) Ansari, S. A.; Husain, Q. Potential Applications of Enzymes Immobilized on/in Nano Materials: A Review. *Biotechnol. Adv.* **2012**, *30*, 512–523.
- (17) Claussen, J. C.; Malanoski, A.; Breger, J. C.; Oh, E.; Walper, S. A.; Susumu, K.; Goswami, R.; Deschamps, J. R.; Medintz, I. L. Probing the Enzymatic Activity of Alkaline Phosphatase within Quantum Dot Bioconjugates. *J. Phys. Chem. C* **2015**, *119*, 2208–2221.
- (18) Brown, C. W., III; Oh, E.; Hastman, J.; Walper, S. A.; Susumu, K.; Stewart, M. H.; Deschamps, J. R.; Medintz, I. L. Kinetic Enhancement of the Diffusion-Limited Enzyme Beta-Galactosidase When Displayed with Quantum Dots. *RSC Adv.* **2015**, *5*, 93089–93094.
- (19) Algar, W. R.; Malanoski, A.; Deschamps, J. R.; Blanco-Canosa, J. B.; Susumu, K.; Stewart, M. H.; Johnson, B. J.; Dawson, P. E.; Medintz, I. L. Proteolytic Activity at Quantum Dot-Conjugates: Kinetic Analysis Reveals Enhanced Enzyme Activity and Localized Interfacial “Hopping”. *Nano Lett.* **2012**, *12*, 3793–3802.

- (20) Wu, M.; Algar, W. R. Acceleration of Proteolytic Activity Associated with Selection of Thiol Ligand Coatings on Quantum Dots. *ACS Appl. Mater. Interfaces* **2015**, *7*, 2535–2545.
- (21) Wu, M.; Petryayeva, E.; Medintz, I. L.; Algar, W. R. Quantitative Measurement of Proteolytic Rates with Quantum Dot–Peptide Substrate Conjugates and Forster Resonance Energy Transfer. In *Quantum Dots: Applications in Biology*, 2nd ed.; Fontes, A., Santos, B. S., Eds.; Humana Press Inc.: Totowa, 2014; Vol. 1199, pp 215–239.
- (22) Wu, M.; Petryayeva, E.; Algar, W. R. Quantum Dot-Based Concentric Fret Configuration for the Parallel Detection of Protease Activity and Concentration. *Anal. Chem.* **2014**, *86*, 11181–11188.
- (23) Zobel, M.; Neder, R. B.; Kimber, S. A. Universal Solvent Restructuring Induced by Colloidal Nanoparticles. *Science* **2015**, *347*, 292–294.
- (24) Pfeiffer, C.; Rehbock, C.; Hühn, D.; Carrillo-Carrion, C.; de Aberasturi, D. J.; Merk, V.; Barcikowski, S.; Parak, W. J. Interaction of Colloidal Nanoparticles with Their Local Environment: The (Ionic) Nanoenvironment around Nanoparticles Is Different from Bulk and Determines the Physico-Chemical Properties of the Nanoparticles. *J. R. Soc., Interface* **2014**, *11*, 20130931.
- (25) Hsu, H.-J.; Sen, S.; Pearson, R. M.; Uddin, S.; Král, P.; Hong, S. Poly(Ethylene Glycol) Corona Chain Length Controls End-Group-Dependent Cell Interactions of Dendron Micelles. *Macromolecules* **2014**, *47*, 6911–6918.
- (26) Pearson, R. M.; Sen, S.; Hsu, H.-j.; Pasko, M.; Gaske, M.; Král, P.; Hong, S. Tuning the Selectivity of Dendron Micelles through Variations of the Poly(Ethylene Glycol) Corona. *ACS Nano* **2016**, *10*, 6905–6914.
- (27) Lin, G.; Chee, S. W.; Raj, S.; Král, P.; Mirsaidov, U. Linker-Mediated Self-Assembly Dynamics of Charged Nanoparticles. *ACS Nano* **2016**, *10*, 7443–7450.
- (28) Yang, M.; Chan, H.; Zhao, G.; Zhang, P.; Král, P.; Kotov, N. A. Self-Assembly of Nanoparticles into Biomimetic Capsid-Like Nano-shells. *Nat. Chem.* **2016**, *9*, 287–294.
- (29) Zhao, Z.; Fu, J.; Dhakal, S.; Johnson-Buck, A.; Liu, M.; Zhang, T.; Woodbury, N. W.; Liu, Y.; Walter, N. G.; Yan, H. Nanocaged Enzymes with Enhanced Catalytic Activity and Increased Stability against Protease Digestion. *Nat. Commun.* **2016**, *7*, 10619.
- (30) Bera, M. K.; Chan, H.; Moyano, D. F.; Yu, H.; Tatur, S.; Amoanu, D.; Bu, W.; Rotello, V. M.; Meron, M.; Kral, P.; Lin, B. H.; Schlossman, M. L. Interfacial Localization and Voltage-Tunable Arrays of Charged Nanoparticles. *Nano Lett.* **2014**, *14*, 6816–6822.
- (31) Zhao, H.; Sen, S.; Udayabhaskararao, T.; Sawczyk, M.; Kucanda, K.; Manna, D.; Kundu, P. K.; Lee, J. W.; Kral, P.; Klajn, R. Reversible Trapping and Reaction Acceleration within Dynamically Self-Assembling Nanoflasks. *Nat. Nanotechnol.* **2016**, *11*, 82–88.
- (32) del Pino, P.; Yang, F.; Pelaz, B.; Zhang, Q.; Kantner, K.; Hartmann, R.; de Baroja, N. M.; Gallego, M.; Möller, M.; Manshian, B. B.; Soenen, S. J.; Riedel, R.; Hampp, N.; Parak, W. J. Basic Physicochemical Properties of Polyethylene Glycol Coated Gold Nanoparticles That Determine Their Interaction with Cells. *Angew. Chem., Int. Ed.* **2016**, *55*, 5483–5487.
- (33) Feliu, N.; Docter, D.; Heine, M.; del Pino, P.; Ashraf, S.; Kolosnjaj-Tabi, J.; Macchiarini, P.; Nielsen, P.; Alloyear, D.; Gazeau, F.; Stauber, R. H.; Parak, W. J. *In Vivo* Degeneration and the Fate of Inorganic Nanoparticles. *Chem. Soc. Rev.* **2016**, *45*, 2440–2457.
- (34) Kreyling, W. G.; Abdelmonem, A. M.; Ali, Z.; Alves, F.; Geiser, M.; Haberl, N.; Hartmann, R.; Hirn, S.; de Aberasturi, D. J.; Kantner, K.; Khadem-Saba, G.; Montenegro, J. M.; Rejman, J.; Rojo, T.; de Larramendi, I. R.; Ufartes, R.; Wenk, A.; Parak, W. J. *In Vivo* Integrity of Polymer-Coated Gold Nanoparticles. *Nat. Nanotechnol.* **2015**, *10*, 619–623.
- (35) Nazarenus, M.; Zhang, Q.; Soliman, M. G.; del Pino, P.; Pelaz, B.; Carregal-Romero, S.; Rejman, J.; Rothen-Rutishauser, B.; Clift, M. J. D.; Zellner, R.; Nienhaus, G. U.; Delehanty, J. B.; Medintz, I. L.; Parak, W. J. *In Vitro* Interaction of Colloidal Nanoparticles with Mammalian Cells: What Have We Learned Thus Far? *Beilstein J. Nanotechnol.* **2014**, *5*, 1477–1490.
- (36) Gemmill, K. B.; Díaz, S. A.; Blanco-Canosa, J. B.; Deschamps, J. R.; Pons, T.; Liu, H.-W.; Deniz, A.; Melinger, J.; Oh, E.; Susumu, K.; Stewart, M. H.; Hastman, D. A.; North, S. H.; Delehanty, J. B.; Dawson, P. E.; Medintz, I. L. Examining the Polyproline Nanoscopic Ruler in the Context of Quantum Dots. *Chem. Mater.* **2015**, *27*, 6222–6237.
- (37) Blanco-Canosa, J.; Wu, M.; Susumu, K.; Petryayeva, E.; Jennings, T. L.; Dawson, P. E.; Algar, W. R.; Medintz, I. L. Recent Progress in the Bioconjugation of Quantum Dots. *Coord. Chem. Rev.* **2014**, *263–264*, 101–137.
- (38) Díaz, S. A.; Breger, J. C.; Medintz, I. L. Monitoring Enzymatic Proteolysis Using Either Enzyme- or Substrate-Bioconjugated Quantum Dots. In *Methods in Enzymology*; Challa Vijaya, K., Ed.; Academic Press, 2016; Vol. 571, pp 19–54.
- (39) Cornish-Bowden, A. *Fundamentals of Enzyme Kinetics*, 4th ed.; Wiley-Blackwell: Weinheim, Germany, 2012.
- (40) Johnson, K. A.; Goody, R. S. The Original Michaelis Constant: Translation of the 1913 Michaelis-Menten Paper. *Biochemistry* **2011**, *50*, 8264–8269.
- (41) Duggleby, R. G. Quantitative Analysis of the Time Courses of Enzyme-Catalyzed Reactions. *Methods* **2001**, *24*, 168–174.
- (42) Eisenthal, R.; Danson, M. J.; Hough, D. W. Catalytic Efficiency and  $k_{cat}/K_m$ : A Useful Comparator? *Trends Biotechnol.* **2007**, *25*, 247–249.
- (43) Susumu, K.; Oh, E.; Delehanty, J. B.; Blanco-Canosa, J. B.; Johnson, B. J.; Jain, V.; Herve, W. J.; Algar, W. R.; Boeneman, K.; Dawson, P. E.; Medintz, I. L. Multifunctional Compact Zwitterionic Ligands for Preparing Robust Biocompatible Semiconductor Quantum Dots and Gold Nanoparticles. *J. Am. Chem. Soc.* **2011**, *133*, 9480–9496.
- (44) Algar, W. R.; Susumu, K.; Delehanty, J. B.; Medintz, I. L. Semiconductor Quantum Dots in Bioanalysis: Crossing the Valley of Death. *Anal. Chem.* **2011**, *83*, 8826–8837.
- (45) Susumu, K.; Oh, E.; Delehanty, J. B.; Pinaud, F.; Gemmill, K. B.; Walper, S.; Breger, J.; Schroeder, M. J.; Stewart, M. H.; Jain, V.; Whitaker, C. M.; Huston, A. L.; Medintz, I. L. A New Family of Pyridine-Appended Multidentate Polymers as Hydrophilic Surface Ligands for Preparing Stable Biocompatible Quantum Dots. *Chem. Mater.* **2014**, *26*, 5327–5344.
- (46) Ikeda, Y.; Nagasaki, Y. PEGylation Technology in Nanomedicine. In *Polymers in Nanomedicine*; Kunugi, S., Yamaoka, T., Eds.; Springer: Berlin, 2012; Vol. 247, pp 115–140.
- (47) Nagasaki, Y. Engineering of Poly(Ethylene Glycol) Chain-Tethered Surfaces to Obtain High-Performance Bionanoparticles. *Sci. Technol. Adv. Mater.* **2010**, *11*, 054505.
- (48) Ulbrich, K.; Hola, K.; Subr, V.; Bakandritsos, A.; Tucek, J.; Zboril, R. Targeted Drug Delivery with Polymers and Magnetic Nanoparticles: Covalent and Noncovalent Approaches, Release Control, and Clinical Studies. *Chem. Rev.* **2016**, *116*, 5338–5431.
- (49) Palui, G.; Aldeek, F.; Wang, W. T.; Mattoussi, H. Strategies for Interfacing Inorganic Nanocrystals with Biological Systems Based on Polymer-Coating. *Chem. Soc. Rev.* **2015**, *44*, 193–227.
- (50) Prasuhn, D. E.; Deschamps, J. R.; Susumu, K.; Stewart, M. H.; Boeneman, K.; Blanco-Canosa, J. B.; Dawson, P. E.; Medintz, I. L. Polyvalent Display and Packing of Peptides and Proteins on Semiconductor Quantum Dots: Predicted *Versus* Experimental Results. *Small* **2010**, *6*, 555–564.
- (51) Phillips, J. C.; Braun, R.; Wang, W.; Gumbart, J.; Tajkhorshid, E.; Villa, E.; Chipot, C.; Skeel, R. D.; Kalé, L.; Schulten, K. Scalable Molecular Dynamics with NAMD. *J. Comput. Chem.* **2005**, *26*, 1781–1802.
- (52) Díaz, S. A.; Malonoski, A. P.; Susumu, K.; Hofele, R. V.; Oh, E.; Medintz, I. L. Probing the Kinetics of Quantum Dot-Based Proteolytic Sensors. *Anal. Bioanal. Chem.* **2015**, *407*, 7307–7318.
- (53) Chiu, K.; Agoubi, L. L.; Lee, I.; Limpar, M. T.; Lowe, J. W.; Goh, S. L. Effects of Polymer Molecular Weight on the Size, Activity, and Stability of PEG-Functionalized Trypsin. *Biomacromolecules* **2010**, *11*, 3688–3692.
- (54) Warshel, A.; Russell, S. Theoretical Correlation of Structure and Energetics in the Catalytic Reaction of Trypsin. *J. Am. Chem. Soc.* **1986**, *108*, 6569–6579.

(55) Bartunik, H. D.; Summers, L. J.; Bartsch, H. H. Crystal Structure of Bovine B-Trypsin at 1.5 Å Resolution in a Crystal Form with Low Molecular Packing Density. *J. Mol. Biol.* **1989**, *210*, 813–828.

(56) Huber, R.; Bode, W. Structural Basis of the Activation and Action of Trypsin. *Acc. Chem. Res.* **1978**, *11*, 114–122.

(57) Huddleston, J. G.; Looney, T. K.; Broker, G. A.; Griffin, S. T.; Spear, S. K.; Rogers, R. D. Comparative Behavior of Poly(Ethylene Glycol) Hydrogels and Poly(Ethylene Glycol) Aqueous Biphasic Systems. *Ind. Eng. Chem. Res.* **2003**, *42*, 6088–6095.

(58) Sapsford, K. E.; Tyner, K. M.; Dair, B. J.; Deschamps, J. R.; Medintz, I. L. Analyzing Nanomaterial Bioconjugates: A Review of Current and Emerging Purification and Characterization Techniques. *Anal. Chem.* **2011**, *83*, 4453–4488.

(59) Sapsford, K. E.; Farrell, D.; Sun, S.; Rasooly, A.; Mattoussi, H.; Medintz, I. L. Monitoring of Enzymatic Proteolysis on a Electroluminescent-Ccd Microchip Platform Using Quantum Dot-Peptide Substrates. *Sens. Actuators, B* **2009**, *139*, 13–21.

(60) Oh, E.; Fatemi, F. K.; Currie, M.; Delehanty, J. B.; Pons, T.; Fragola, A.; Leveque-Fort, S.; Goswami, R.; Susumu, K.; Huston, A. L.; Medintz, I. L. PEGylated Luminescent Gold Nanoclusters: Synthesis, Characterization, Bioconjugation, and Application to One- and Two-Photon Cellular Imaging. *Part. Part. Syst. Character.* **2013**, *30*, 453–466.

(61) Algar, W. R.; Blanco-Canosa, J. B.; Manthe, R. L.; Susumu, K.; Stewart, M. H.; Dawson, P. E.; Medintz, I. L. Synthesizing and Modifying Peptides for Chemoselective Ligation and Assembly into Quantum Dot-Peptide Bioconjugates. In *Nanomaterial Interfaces in Biology: Methods and Protocols*; Bergese, P., HamadSchifferli, K., Eds.; Springer: Berlin, 2013; Vol. 1025, pp 47–73.

(62) Medintz, I.; Hildebrandt, N. *FRET—Förster Resonance Energy Transfer: From Theory to Applications*; Wiley-VCH Verlag GmbH: Weinheim, Germany, 2014.

(63) Hildebrandt, N.; Spillmann, C. M.; Algar, W. R.; Pons, T.; Stewart, M. H.; Oh, E.; Susumu, K.; Díaz, S. A.; Delehanty, J. B.; Medintz, I. L. Energy Transfer with Semiconductor Quantum Dot Bioconjugates: A Versatile Platform for Biosensing, Energy Harvesting, and Other Related Applications. *Chem. Rev.* **2017**, *117*, 536–711.

(64) Lakowicz, J. R. *Principles of Fluorescence Spectroscopy*, 3rd ed.; Springer: New York, 2006.

(65) Walter, J.; Steigemann, W.; Singh, T. P.; Bartunik, H.; Bode, W.; Huber, R. On the Disordered Activation Domain in Trypsinogen - Chemical Labeling and Low-Temperature Crystallography. *Acta Crystallogr., Sect. B: Struct. Crystallogr. Cryst. Chem.* **1982**, *38*, 1462–1472.

(66) Vanommeslaeghe, K.; Hatcher, E.; Acharya, C.; Kundu, S.; Zhong, S.; Shim, J.; Darian, E.; Guvench, O.; Lopes, P.; Vorobyov, I.; MacKerell, A. D. Charmm General Force Field (Cgenff): A Force Field for Drug-Like Molecules Compatible with the Charmm All-Atom Additive Biological Force Fields. *J. Comput. Chem.* **2010**, *31*, 671–690.

(67) Yu, W.; He, X.; Vanommeslaeghe, K.; MacKerell, A. D. Extension of the Charmm General Force Field to Sulfonyl-Containing Compounds and Its Utility in Biomolecular Simulations. *J. Comput. Chem.* **2012**, *33*, 2451–2468.

(68) MacKerell, A. D.; Bashford, D.; Bellott, M.; Dunbrack, R. L.; Evanseck, J. D.; Field, M. J.; Fischer, S.; Gao, J.; Guo, H.; Ha, S.; Joseph-McCarthy, D.; Kuchnir, L.; Kuczera, K.; Lau, F. T. K.; Mattos, C.; Michnick, S.; Ngo, T.; Nguyen, D. T.; Prodhom, B.; Reiher, W. E.; et al. All-Atom Empirical Potential for Molecular Modeling and Dynamics Studies of Proteins. *J. Phys. Chem. B* **1998**, *102*, 3586–3616.

(69) Best, R. B.; Zhu, X.; Shim, J.; Lopes, P. E. M.; Mittal, J.; Feig, M.; MacKerell, A. D. Optimization of the Additive Charmm All-Atom Protein Force Field Targeting Improved Sampling of the Backbone  $\Phi$ ,  $\Psi$  and Side-Chain X(1) and X(2) Dihedral Angles. *J. Chem. Theory Comput.* **2012**, *8*, 3257–3273.

(70) Darden, T.; York, D.; Pedersen, L. Particle Mesh Ewald: An N-Log(N) Method for Ewald Sums in Large Systems. *J. Chem. Phys.* **1993**, *98*, 10089–10092.